bonds, $J_{^{107}Ag-P}$ = 601 Hz.[62] Addition of **4** to a solution of **8** produced broadened spectra at room temperature, suggesting that exchange of $AgPPh_3^+$ between $[Ir(H)_2(bpy)(PPh_3)_2]^+$ groups was occurring. Furthermore, addition of **5** to solutions of **8** also produced broadened spectra, which suggested that exchange of PPh_3 between $[AgIr(H)_2(bpy)(PPh_3)_2]^{2+}$ groups occurred as well. Infrared and conductivity data for **8** were consistent with the formulation of a 1:2 electrolyte.

Complex **8** reacted further with PPh_3 to produce homometallic Ir and Ag fragments. When a slight excess of PPh_3 was added to **8** and dissolved in CH_2Cl_2, the $^{31}P\{^1H\}$ NMR spectrum showed a singlet at δ 18.7 and two doublets centered at δ 8.3 (J = 367, 318 Hz). This is consistent with the formation of $[Ir(H)_2(bpy)(PPh_3)_2]^+$ (**4**) and $Ag(PPh_3)_3^+$.[61] Nucleophilic attack of PPh_3 on M–$AuPPh_3$ or M–$AgPPh_3$ to produce M and $M'(PPh_3)_x^+$ is a common reaction.[2,63]

Summary. Several new heterobimetallic hydrides containing Au or Ag have been synthesized. $[AuRu(H)_2(dppm)_2(PPh_3)]PF_6$ (**3**) was characterized by ^{31}P and ^1H NMR spectroscopy and single-crystal X-ray crystallography. The hydride positions were located, refined, and determined to be bridging the Ru–Au bond. ^{31}P and ^1H NMR spectroscopy provided further support for this bridging dihydride formulation due to large spin–spin coupling between the hydride ligands and the gold phosphine phosphorus atom. The bridging dihydride formulation for the previously characterized $[AuIr(H)_2(bpy)(PPh_3)_3](BF_4)_2$ (**2**)[2] was further substantiated by comparing the Ir–N bond lengths in **2** to those in $[Ir(H)_2(bpy)(PPh_3)_2]PF_6$ (**4**). The average Ir–N bond length in **2** is significantly shorter than in **4**. It was argued that this is due to the weaker structural trans influence of bridging hydrides in **2** compared with the stronger influence of the terminal hydrides in **4**.

Stable 1:1 adducts of the BF_4^- salt of **4** were synthesized, including $[AgIr(H)_2(bpy)(PPh_3)_2](O_3SCF_3)(BF_4)$ (**5**), $[AgIr(H)_2(bpy)(PPh_3)_2(NO_3)](BF_4)$ (**6**), $[AuIr(H)_2(bpy)(PPh_3)_2(CH_3CN)](BF_4)_2$ (**7**), and $[AgIr(H)_2(bpy)(PPh_3)_3](O_3SCF_3)(BF_4)$ (**8**). Complexes **5–7** are interesting in that they contain labile ligands bound to the coinage metal. The ability of the group 1B metal to provide open coordination sites near a transition-metal hydride may find use in homogeneous catalysis, since evidence for catalyst improvement upon incorporation of a group 1B metal into a transition-metal cluster has been reported.[33] Complexes **5–8** were characterized by IR and ^{31}P and ^1H NMR spectroscopy and determined to have the bridging dihydride formulation in the solid state analogous to the case for **2** and **3**. In solution, however, the IrAg complexes were shown to be kinetically labile while the IrAu complexes were not. It was also found that only 1:1 adducts were formed and the hydrides were not replaced by Au or Ag. This may be due to the presence of the bpy ligand since Au_2Ir complex formation and H^+ loss occurred when the ligand trans to the hydride was a nitrate,[5] a stronger trans-effect ligand. Also, in the case of Ag, Ag–Ag bonds are not nearly as common as Au–Au bonds, and evidence suggests that Ag is more likely to bind to hydrides rather than replace them. Steric hindrance may also be a contributing factor due to the large size of the bpy and PPh_3 ligands.

Acknowledgment. This work has been supported by the National Science Foundation (Grant CHE-851923) and by the donors of the Petroleum Research Fund, administered by the American Chemical Society. We also thank the Johnson Matthey Co. for generous loans of salts of gold and iridium. B.D.A. thanks General Electric for an industrial fellowship.

Supplementary Material Available: ORTEP drawings of **3** and **4**, the ^1H NMR spectrum of the hydride resonances of **3** with selective ^{31}P decoupling, and listings of general temperature factor expressions, final positional and thermal parameters for all atoms including counterions, solvate molecules, and calculated hydrogen atom positions, least-squares planes, and distances and angles of **3** and **4** (35 pages); listings of observed and calculated structure factor amplitudes of **3** and **4** (58 pages). Ordering information is given on any current masthead page.

(62) Salter, I. D.; Stone, F. G. A. *J. Organomet. Chem.* **1984**, *260*, C71.
(63) Alexander, B. D.; Boyle, P. D.; Johnson, B. J.; Casalnuovo, J. A.; Johnson, S. M.; Mueting, A. M.; Pignolet, L. H. *Inorg. Chem.* **1987**, *26*, 2547.
(64) The periodic group notation in parentheses is in accord with recent actions by IUPAC and ACS nomenclature committees. A and B notation is eliminated because of wide confusion. Groups IA and IIA become groups 1 and 2. The d-transition elements comprise groups 3 through 12, and the p-block elements comprise groups 13 through 18. (Note that the former Roman number designation is preserved in the last digit of the numbering: e.g., III → 3 and 13.)

Contribution from the School of Chemistry, University of New South Wales, Kensington, NSW 2033, Australia

Magnetic, Spectroscopic, and Structural Characterization of Singlet ⇌ Quintet Transitions in Iron(II) Complexes of Methyl-Substituted Pyridinylthiazoles

Anthony T. Baker,[1] Harold A. Goodwin,* and A. David Rae*

Received February 24, 1987

Iron(II) and nickel(II) $[ML_3]X_2$ type complexes have been prepared where L = 2-methyl-4-(pyridin-2-yl)thiazole (2mpt), 4-methyl-2-(pyridin-2-yl)thiazole (4mpt), and 2-(6-methylpyridin-2-yl)thiazole (6mpt). Salts of both $[Fe(2mpt)_3]^{2+}$ and $[Fe(4mpt)_3]^{2+}$ have strongly temperature-dependent magnetic moments that indicate the occurrence of a singlet ($^1A_1$) ⇌ quintet ($^5T_2$) spin transition. This is confirmed by Mössbauer and electronic spectral data. $[Fe(6mpt)_3][ClO_4]_2$ is a purely high-spin species. The spin transition in $[Fe(4mpt)_3][ClO_4]_2$ is fairly abrupt and virtually complete within the range 100–300 K. The structure of this complex has been determined at 294 and 133 K. The change in temperature is accompanied by a contraction in the average Fe–N distance of 0.16 Å and a disorder–order transition in the anion orientation. Nickel complexes were prepared to allow comparisons of ligand field and structural characteristics. The structure of $[Ni(4mpt)_3][ClO_4]_2$ was determined at 294 K. Crystal data: $[Fe(4mpt)_3][ClO_4]_2$ at 294 K, space group $P\bar{3}c1$, $a = b$ = 10.223 (2) Å, c = 17.782 (6) Å, $\alpha = \beta$ = 90°, γ = 120°, Z = 2; $[Fe(4mpt)_3][ClO_4]_2$ at 133 K, space group $P\bar{3}c1$, $a = b$ = 10.145 (7) Å, c = 17.39 (1) Å, $\alpha = \beta$ = 90°, γ = 120°, Z = 2; $[Ni(4mpt)_3][ClO_4]_2$ at 294 K, space group $P\bar{3}c1$, $a = b$ = 10.246 (1) Å, c = 17.627 (3) Å, $\alpha = \beta$ = 90°, γ = 120°, Z = 2.

Introduction

Electronic spin-state transitions in iron(II) (d^6) systems can be generated in a number of ways, but one of the most effective is to modify structurally the strong-field diimine systems 2,2-bipyridine (bpy) or 1,10-phenanthroline (phen) so that the reduced field strength lies near the critical value where the quintet/singlet crossover occurs.[2] This is illustrated for example by the replacement of one pyridyl group in bpy by an imidazolyl to give 2-(pyridin-2-yl) imidazole (pyi). The spin transition in salts of

(1) CSIRO, Division of Protein Chemistry, Parkville, 3052 Victoria, Australia.
(2) Goodwin, H. A. *Coord. Chem. Rev.* **1976**, *18*, 293.

0020-1669/87/1326-3513$01.50/0

$[Fe(pyi)_3]^{2+}$ has been well characterized in both the solid state and in solution.[3-6] An alternative, and equally effective strategy, is the incorporation of a methyl group into the 2-position of 1,10-phenanthroline. This introduces a strong steric barrier to close approach of a metal ion and salts of $[Fe(mephen)_3]^{2+}$ are high-spin at room temperature but undergo a reversible quintet→singlet transition as the temperature is lowered.[7,8] The difference in the spin states of $[Fe(phen)_3]^{2+}$ and $[Fe(mephen)_3]^{2+}$ is reflected in the differences in the Fe–N distances. In the former (low-spin) complex the average distance is 1.97 Å,[9] whereas in the latter (high spin at room temperature) species it is 2.23 Å.[10] This relatively large difference in bond length is fairly typical for iron(II) with change in spin state, but its significance is greater when it is measured for the one system in two spin states, which effectively means structure determination at more than one temperature. This has been reported in a few instances,[11] most notably in the detailed structural studies of salts of the tris(2-picolylamine)iron(II) cation.[12-14] Such studies are valuable not only for quantifying the intramolecular changes associated with a spin transition but also as an aid in the understanding of the effects of solid-state forces on the course of a spin transition.

In earlier work[15,16] we have shown that the incorporation of a thiazolyl moiety into the bipyridine system, in contrast to an imidazolyl, does not affect the spin state of the $[FeN_6]^{2+}$ complex, despite the reduced stability of the complexes in solution, compared with that of $[Fe(bpy)_3]^{2+}$.[17] In the present work we report the effect of an additional modification, i.e. the incorporation of a methyl substituent adjacent to a donor atom in the 4-(pyridin-2-yl)- and 2-(pyridin-2-yl)thiazole systems, this representing a combination of the two approaches mentioned above. The three ligand systems 2-methyl-4-(pyridin-2-yl)thiazole (2mpt) (**1**), 4-methyl-2-(pyridin-2-yl)thiazole (4mpt) (**2**) and 2-(6-methylpyridin-2-yl)thiazole (6mpt) (**3**) are considered.

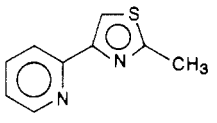

1

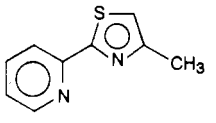

2

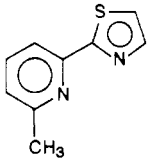

3

Experimental Section

Preparations. 4-Methyl-2-(pyridin-2-yl)thiazole was prepared by the method of Karrer and Schukri,[18] except that bromoacetone was used instead of chloroacetone. 2-Methyl-4-(pyridin-2-yl)thiazole was obtained by the method of Glover and Thomas.[19] 2-(6-Methyl-pyridin-2-yl)-thiazole was prepared by the following method. 6-Methyl-2-thiopicolinamide (Aldrich) (9.3 g, 61 mmol) and bromoacetal (12 g, 61 mmol) were heated together on a steam bath for 16 h. The reaction mixture was cooled, and the tarry residue was washed with ether (3 × 25 mL). It was then dissolved in hydrochloric acid (30 mL, 1 M). The solution was filtered and then basified with K_2CO_3. The mixture was extracted with ether (3 × 50 mL), the combined extracts were dried over anhydrous sodium sulfate, and the ether was distilled off. The brown oily residue was purified by chromatography on alumina with ether as eluent. The product was obtained by evaporation of the ether and recrystallization from light petroleum. It was obtained as a very low melting (m.p. ≅ 25 °C) hygroscopic solid, which analyzed satisfactorily as a hemihydrate. The complexes were all prepared by the direct interaction of hot ethanolic solutions of the ligand and the appropriate metal salt (ligand:metal molar ratio 3:1). The products crystallized when the reaction mixture was cooled. They were washed with ethanol and dried in vacuo. Satisfactory analytical data were obtained for all complexes. These are collected in Table SI. Yields of complexes were almost quantitative, and the perchlorate salts were prepared in amounts not exceeding 0.5 g.

Table I. Crystallographic Data for $[M(4mpt)_3][ClO_4]_2$

	M = Fe	M = Fe	M = Ni
formula	$C_{27}H_{24}Cl_2FeN_6O_8S_3$	$C_{27}H_{24}Cl_2FeN_6O_8S_3$	$C_{27}H_{24}Cl_2NiN_6O_8S_3$
fw	783.46	783.46	786.32
T, K	294	133	294
cryst class	trigonal	trigonal	trigonal
space group	$P\bar{3}c1$	$P\bar{3}c1$	$P\bar{3}c1$
Z	2	2	2
a, Å	10.223 (2)	10.145 (7)	10.246 (1)
b, Å	10.223 (2)	10.145 (7)	10.246 (1)
c, Å	17.782 (6)	17.39(1)	17.627 (3)
α, deg	90	90	90
β, deg	90	90	90
γ, deg	120	120	120
V, Å^3	1609.4 (6)	1550 (3)	1602.4 (4)
ρ_m, g cm^{-3}	1.610		1.627
ρ_c, g cm^{-3}	1.617		1.630
radiation	Mo Kα	Mo Kα	Cu Kα
λ, Å	0.710 69	0.710 69	1.541 78
μ, cm^{-1}	8.8	8.8	47.4
$2\theta_{max}$, deg	50	46	120
no. of unique reflctns	946	733	800
no. of obsd reflcns	572	286	661
no. of var params	53[a]	64[b]	53[a]
final R[c]	0.037[a]	0.046	0.045[a]
final R_w[d]	0.044[a]	0.057	0.076[a]
$F(000)$	800	800	804

[a] The Fourier back-transform technique has been applied to these values to subtract the effect of the residual perchlorate scattering density. R factors about 0.010 higher were obtained by using 22 additional variables to describe the anion. [b] Slack constraints allow 69 variables to describe 64 independent variables. [c] $R = \sum||F_o| - |F_c||/\sum|F_o|$. [d] $R_w = [\sum_w||F_o| - |F_c||^2/\sum_w|F_o|^2]^{1/2}$.

Physical Measurements. Magnetic data for solid samples were obtained with a variable-temperature Newport Instruments' Gouy system. The field strength was calibrated with $CoHg(NCS)_4$. Magnetic susceptibilities were corrected for diamagnetism by using Pascal's constants.[20] Molar susceptibilities are given in m^3 mol^{-1}, and magnetic moments were calculated according to the relation $\mu = 798(\chi_M T)^{1/2}$. Magnetic data for samples in solution were obtained by the Evans method.[21]

Mössbauer spectral data were obtained with a scanned velocity spectrometer operating in the time mode, equipped with a 10 mCi palladium matrix source at room temperature and calibrated with metallic iron foil. The spectral parameters were obtained from a least-squares fitting to Lorentzian line shapes. Isomer shifts are quoted on the standard iron scale; for conversion to the nitroprusside scale add 0.257 mm s^{-1}.

Electronic spectra for both solids and solutions were obtained with a Zeiss PMQII spectrophotometer equipped with a diffuse reflectance accessory and calibrated with magnesium oxide. The low-temperature reflectance spectra were obtained with a brass attachment containing silica glass windows which was in contact with liquid nitrogen. The

(3) Dosser, R. J.; Eilbeck, W. J.; Underhill, A. E.; Edwards, P. R.; Johnson, C. E. *J. Chem. Soc. A* **1969**, 810.
(4) Reeder, K. A.; Dose, E. V.; Wilson, L. J. *Inorg. Chem.* **1978**, *17*, 1071.
(5) McGarvey, J. J.; Lawthers, I.; Heremans, K.; Toftlund, H. *J. Chem. Soc., Chem. Commun.* **1984**, 1575.
(6) DiBenedetto, J.; Arkle, V.; Goodwin, H. A.; Ford, P. C. *Inorg. Chem.* **1985**, *24*, 455.
(7) Goodwin, H. A.; Sylva, R. N. *Aust. J. Chem.* **1968**, *21*, 1081.
(8) König, E.; Ritter, G.; Braunecker, B.; Madeja, K.; Goodwin, H. A.; Smith, F. E. *Ber. Bunsen-Ges. Phys. Chem.* **1972**, *76*, 393.
(9) Johansson, L.; Molund, M.; Oskarsson, A. *Inorg. Chim. Acta* **1978**, *31*, 117.
(10) Goodwin, H. A.; Kucharski, E. S.; White, A. H. *Aust. J. Chem.* **1983**, *36*, 1115.
(11) König, E. *Prog. Inorg. Chem.*, in press.
(12) Katz, B. A.; Strouse, C. E. *Inorg. Chem.* **1980**, *19*, 658.
(13) Katz, B. A.; Strouse, C. E. *J. Am. Chem. Soc.* **1979**, *101*, 6214.
(14) Mikami, M.; Konno, M.; Saito, Y. *Acta Crystallogr., Sect. B: Struct. Crystallogr. Cryst. Chem.* **1980**, *B36*, 275.
(15) Fitzpatrick, L. J.; Goodwin, H. A. *Inorg. Chim. Acta* **1982**, *61*, 229.
(16) Baker, A. T.; Goodwin, H. A.; Rae, A. D. *Aust. J. Chem.* **1984**, *37*, 2431.
(17) Eilbeck, W. J.; Holmes, F.; Thomas, T. W.; Williams, G. *J. Chem. Soc. A* **1968**, *2348*.
(18) Karrer, P.; Schukri, J. *Helv. Chim. Acta* **1945**, *28*, 820.
(19) Glover, E. E.; Thomas, T. R. *J. Chem. Soc. C* **1967**, *463*.
(20) Figgis, B. N.; Lewis, J. *Modern Coordination Chemistry*; Lewis, J., Wilkins, R. G., Eds.; Interscience: New York, 1960.
(21) Evans, D. F. *J. Chem. Soc.* **1959**, 2003.

Table II. Positional Parameters for $[Fe(4mpt)_3][ClO_4]_2$ at 294 K

atom	x	y	z	U_{eq},[a] Å^2
Fe	0.00000	0.00000	0.25000	0.053 (1)
N(1)	0.1474 (6)	0.2166 (8)	0.3042 (3)	0.057 (2)
S(1)	0.3940 (2)	0.4685 (2)	0.3045 (1)	0.086 (2)
C(12)	0.2735 (5)	0.2998 (5)	0.2656 (3)	0.056 (1)
C(14)	0.1488 (9)	0.2922 (7)	0.3672 (3)	0.070 (1)
C(15)	0.2719 (10)	0.4301 (8)	0.3777 (4)	0.075 (2)
C(Me)	0.0165 (9)	0.2257 (10)	0.4169 (4)	0.086 (2)
N(2)	0.2052 (7)	0.0984 (6)	0.1804 (3)	0.055 (1)
C(22)	0.3009 (7)	0.2421 (8)	0.1958 (3)	0.055 (1)
C(23)	0.4223 (7)	0.3288 (9)	0.1478 (4)	0.066 (2)
C(24)	0.4456 (8)	0.2690 (9)	0.0843 (4)	0.080 (2)
C(25)	0.3454 (8)	0.1199 (9)	0.0690 (3)	0.080 (2)
C(26)	0.2308 (8)	0.0438 (9)	0.1185 (4)	0.066 (1)
Cl	0.3243 (18)	0.6467 (18)	0.1011 (5)	0.122 (10)
O(1)	0.4629 (22)	0.7564 (18)	0.1200 (15)	0.354 (12)
O(2)	0.2524 (23)	0.5677 (19)	0.1625 (8)	0.173 (18)
O(3)	0.2472 (18)	0.7077 (19)	0.0710 (16)	0.343 (23)
O(4)	0.3348 (21)	0.5549 (18)	0.0509 (16)	0.266 (18)

[a] $U_{eq} = {}^1/_3(U_{11} + U_{22} + U_{33})$ where U_{ij} values are defined relative to orthonormal axes parallel to a, b^*, and c.

fitting was sealed from the atmosphere, and a stream of dry nitrogen gas was passed over the window surfaces to prevent water condensation.

Crystal Structure Determination for $[M(4mpt)_3][ClO_4]_2$. Crystal data and details of the data collection, solution, and refinement of the three structures are given in Table I. Data were collected at 294 K by means of an Enraf Nonius CAD4 automatic four-circle diffractometer. The low-temperature data were collected at the University of Wisconsin, Madison, WI, by using a Syntex P1 diffractometer. The crystal was cooled by a cold gas stream. The low-temperature data were not corrected for absorption, but the data obtained for both the iron and nickel complexes at 294 K were corrected.[22] Distances from crystal faces to an internal origin: (Fe(294 K), [Ni]) (001) 0.060 [0.241], (0,0,−1) 0.060 [0.224], (0−1,0) 0.103 [0.069], (010) 0.122 [0.060], (100) 0.103 [0.052], (−1,0,0) 0.120 [0.069], (1,−1,0) 0.103 [0.086], (−1,1,0) 0.120 [0.071] mm. The structure of the nickel complex was solved by phasing off partial structures, using as an initial model the metal atom at the 32 site in space group $P\bar{3}c1$ (No. 165). Refinement of the iron structures utilized the final parameters for the nickel complex as the starting point, except that the anion was relocated from difference maps.

Refinement was carried out by using constrained full-matrix least-squares methods (RAELS).[23] Reflection weights used were $1/\sigma^2(F_o)$, being derived from $\sigma[I_o] = [\sigma^2(I_o) + (0.04I_o)^2]^{1/2}$. In each of the three structures each heterocyclic ring of the ligand was constrained to planarity. No constraints were applied to the angle between the planes defined by the two heterocyclic rings of each ligand molecule. The methyl groups were not constrained to the plane of the thiazolyl ring and were found to be 0.076, 0.094, and 0.103 Å out of the plane for the Fe(294 K), Fe(133 K), and Ni complexes, respectively. Rigid-body thermal parametrization (TLX) was applied to the ligands and anions in each structure. The metal atom was modeled as an individual anisotropic atom (with symmetry restrictions for the special position), and the sulfur atom of the thiazolyl ring was allowed further anisotropic thermal motion in addition to the rigid body contribution. Constraints were necessary as the ligands are disordered about the 2-fold axes of $P\bar{3}c1$.

For the Fe(294 K) and Ni structures the anion was found to be disordered about a 3-fold axis. The residual electron density in the region of the anion could not be fully rationalized in terms of a 3-fold disordering of an anion of tetrahedral symmetry at a general position. The Fourier Back-transform technique[24] was applied: the contribution of the residual electron density within 2.5 Å of the Cl atom to each reflection was subsequently added to the model. Further refinement of the cation structure and more realistic errors were obtained as a result. However, this amounted to reductions in the R factor on the order of only 0.01, indicating that residual electron density about the perchlorate ion was not an excessively large systematic error.

For the iron complex at 133 K, the perchlorate ion had two orientations of crystallographic C_{3v} symmetry but these were restrained to T_d symmetry by holding the bond angle to 109.5° and restraining the Cl–O bond lengths for both orientations of the anion to equality. The final occupancies of the two orientations were 0.728 (9) and 0.272 (9). The Cl–O bond length was 1.405 (2) Å.

Convergence of the refinement was obtained by applying planarity and rigid-body thermal motion constraints. However, consistency of ligand structure for the three determinations was not obtained. The deviations were not chemically significant but were a result of ligand disorder. A weighted-average intraligand geometry was determined taking $1/\sigma^2$ as weights where σ is the estimated standard deviation for an observation. The intraligand distances were subsequently constrained to this average, and no significant differences in residuals (R, R_w) were observed.

The final positional parameters for the non-hydrogen atoms are listed in Tables II–IV; thermal parameters are given in Tables SII–SIV. Positional parameters for the hydrogen atoms are given in Table SV.

Table III. Positional Parameters for $[Fe(4mpt)_3][ClO_4]_2$ at 133 K

atom	x	y	z	U_{eq}, Å^2
Fe	0.00000	0.00000	0.25000	0.040 (1)
N(1)	0.1298 (17)	0.2030 (19)	0.3029 (8)	0.041 (3)
S(1)	0.3741 (5)	0.4587 (4)	0.3069 (3)	0.062 (5)
C(12)	0.2593 (12)	0.2883 (13)	0.2653 (6)	0.040 (3)
C(14)	0.1227 (19)	0.2765 (16)	0.3667 (7)	0.050 (4)
C(15)	0.2443 (20)	0.4166 (17)	0.3788 (10)	0.051 (4)
C(Me)	−0.0149 (19)	0.2088 (21)	0.4146 (10)	0.065 (6)
N(2)	0.1899 (15)	0.0833 (13)	0.1829 (8)	0.041 (3)
C(22)	0.2921 (15)	0.2278 (17)	0.1962 (8)	0.041 (3)
C(23)	0.4178 (16)	0.3093 (22)	0.1479 (11)	0.049 (4)
C(24)	0.4411 (17)	0.2438 (18)	0.0851 (8)	0.058 (5)
C(25)	0.3357 (17)	0.0941 (19)	0.0710 (8)	0.056 (5)
C(26)	0.2179 (17)	0.0256 (20)	0.1214 (8)	0.046 (4)
Cl	0.3333	0.6667	0.0976 (3)	0.089 (4)
O(1)	0.3333	0.6667	0.1784 (6)	0.253 (11)
O(2)	0.3454 (12)	0.5425 (10)	0.0705 (4)	0.166 (10)
Cl*	0.3333	0.6667	0.1222 (9)	0.114 (4)
O(1*)	0.3333	0.6667	0.0416 (10)	0.123 (4)
O(2*)	0.2138 (32)	0.5276 (24)	0.1493 (10)	0.241 (11)

Table IV. Positional Parameters for $[Ni(4mpt)_3][ClO_4]_2$

atom	x	y	z	U_{eq}, Å^2
Ni	0.00000	0.00000	0.25000	0.053 (1)
N(1)	0.1372 (8)	0.2097 (9)	0.3042 (4)	0.057 (2)
S(1)	0.3816 (3)	0.4615 (2)	0.3059 (2)	0.084 (3)
C(12)	0.2645 (6)	0.2924 (7)	0.2665 (3)	0.055 (2)
C(14)	0.1326 (10)	0.2839 (9)	0.3670 (4)	0.070 (2)
C(15)	0.2546 (12)	0.4216 (10)	0.3773 (5)	0.076 (2)
C(Me)	−0.0037 (10)	0.2173 (11)	0.4139 (5)	0.086 (3)
N(2)	0.1983 (8)	0.0926 (7)	0.1816 (4)	0.053 (2)
C(22)	0.2958 (8)	0.2354 (8)	0.1970 (4)	0.055 (2)
C(23)	0.4202 (8)	0.3235 (10)	0.1509 (5)	0.065 (2)
C(24)	0.4412 (9)	0.2592 (10)	0.0879 (4)	0.077 (2)
C(25)	0.3404 (8)	0.1110 (10)	0.0717 (4)	0.076 (2)
C(26)	0.2233 (8)	0.0355 (10)	0.1202 (4)	0.062 (2)
Cl	0.3210 (17)	0.6458 (28)	0.0993 (3)	0.122 (8)
O(1)	0.4530 (22)	0.7708 (3)	0.1161 (14)	0.325 (8)
O(2)	0.2546 (23)	0.5710 (6)	0.1639 (5)	0.164 (8)
O(3)	0.2293 (29)	0.6856 (28)	0.0637 (25)	0.306 (7)
O(4)	0.3471 (22)	0.5557 (25)	0.0533 (15)	0.188 (8)

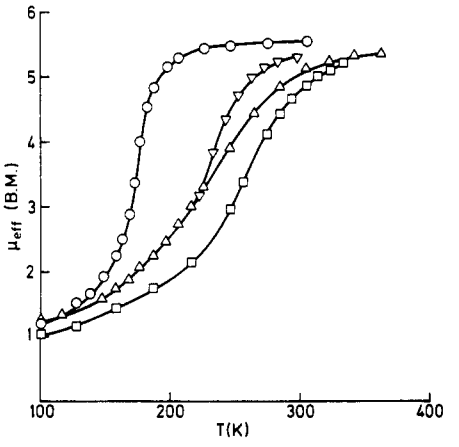

Figure 1. Temperature dependence of the magnetic moment: (○) $[Fe(4mpt)_3][ClO_4]_2$ (solid); (▽) $[Fe(2mpt)_3][BF_4]_2$ (acetone solution); (△) $[Fe(4mpt)_3][BF_4]_2$ (solid); (□) $[Fe(2mpt)_3][ClO_4]_2 \cdot H_2O$ (solid).

(22) Busing, W. R.; Levy, H. A. *Acta Crystallogr.* **1957**, *10*, 180.
(23) Rae, A. D. "RAELS84", University of New South Wales, 1984.
(24) Rae, A. D.; Baker, A. T. *Acta Crystallogr., Sect. A: Found. Crystallogr.* **1984**, *A40*, C428.

Table V. Magnetic Data for Iron Complexes $[FeL_3]X_2 \cdot nH_2O$

T, K	$10^{10}\chi_M$, m^3 mol^{-1}	μ_{eff}, μ_B	T, K	$10^{10}\chi_M$, m^3 mol^{-1}	μ_{eff}, μ_B
	L = 4mpt; X = ClO_4; n = 0 (Solid)				
305	1579	5.54	172.5	1043	3.38
275	1741	5.52	168	780	2.89
246	1928	5.49	163	602	2.50
226	2055	5.44	158.5	504	2.26
206	2142	5.30	148	392	1.92
197	2132	5.17	138	315	1.66
187	1995	4.87	127.6	277	1.50
182	1778	4.54	99	213	1.16
177	1417	4.00			
	L = 4mpt; X = BF_4; n = 0 (Solid)				
363	1254	5.38	206	568	2.73
343	1308	5.34	197	492	2.48
323	1336	5.24	187	431	2.26
305	1350	5.12	177	383	2.08
285	1299	4.85	168	332	1.88
265	1176	4.45	158.5	298	1.73
246	972	3.90	148	265	1.58
226	756	3.30	117	243	1.34
216	665	3.02	99	241	1.23
	L = 4mpt; X = BF_4; n = 0 (Solution)				
293	1548	5.37	253	1797	5.38
283	1586	5.34	243	1888	5.40
273	1664	5.38	233	1974	5.41
263	1699	5.33	223	2068	5.42
	L = 2mpt; X = BF_4; n = 0 (Solution)				
298	1482	5.30	253	1376	4.71
283	1515	5.22	243	1229	4.36
273	1516	5.13	233	978	3.81
263	1486	4.99	223	713	3.18
	L = 2mpt; X = ClO_4; n = 1 (Solid)				
333	1274	5.20	256	703	3.38
323	1266	5.10	246	560	2.96
314	1251	5.00	216	329	2.13
305	1222	4.87	187	260	1.76
294	1156	4.65	158.5	199	1.41
285	1077	4.42	127.6	168	1.17
275	972	4.12	99	173	1.04
	L = 2mpt; X = BF_4; n = 0 (Solid)				
343	1285	5.30	246	650	3.19
333	1289	5.27	236	490	2.71
324	1283	5.14	226	381	2.34
314	1271	5.04	216	306	2.05
305	1257	4.94	206	234	1.75
295	1224	4.79	187	165	1.40
285	1176	4.61	158.5	143	1.20
275	1079	4.34	127.6	121	0.99
265	947	4.00	100	96	0.78
256	808	3.63			
	X = 6mpt; X = ClO_4; n = 1 (Solid)				
305	1631	5.62	187	2674	5.64
275	1800	5.61	158.5	3161	5.65
246	2028	5.63	127.6	3844	5.59
216	2301	5.62	99	4944	5.58

Observed and calculated structure factors are given in Tables SVI–SVIII.

Results and Discussion

Salts of $[Fe(4mpt)_3]^{2+}$ and $[Fe(2mpt)_3]^{2+}$ have magnetic moments that are strongly temperature dependent (Table V and Figure 1), indicative of a thermally induced singlet ($^1A_1$) $\rightleftharpoons$ quintet ($^5T_2$) transition. The transition in $[Fe(4mpt)_3][ClO_4]_2$ is fairly abrupt though it would not be classified as discontinuous. Discontinuous transitions are generally observed for systems in which the spin transition is accompanied by a first-order phase transition, and hysteresis is frequently associated with such transitions.[25] No hysteresis effects were observed in any of the present systems. An order $\rightarrow$ disorder transition involving the perchlorate anion does, however, accompany the singlet $\rightarrow$ quintet transition in $[Fe(4mpt)_3][ClO_4]_2$. This is discussed later. For the other salts the spin transition is more gradual and would clearly be classified as continuous.[26]

No spin pairing was observed in $[Fe(6mpt)_3][ClO_4]_2$ even at the lowest limit of the experimental temperature range. The methyl group adjacent to the pyridine nitrogen atom apparently interferes with the close approach to the metal atom necessary for spin pairing to a greater extent than the group adjacent to the thiazole nitrogen atom in either 2mpt or 4mpt. This is probably due to the particular geometry of the five-membered ring, which directs the substituent somewhat away from the metal ion. Similar effects are observed in the pyridyl–imidazole systems. 2-(Pyridin-2-yl)benzimidazole, in which the fused benzene ring can be expected to exert a steric barrier to coordination not too different from that of a methyl group, is able to effect spin pairing in iron(II) at low temperatures,[27] but 2-(6-methyl-pyridin-2-yl)imidazole yields a purely high-spin complex.[28]

Mössbauer Spectra. Mössbauer spectral data confirm the occurrence of a spin transition in $[Fe(4mpt)_3][ClO_4]_2$ and $[Fe(2mpt)_3][ClO_4]_2$. The spectrum of the former salt shows a single quadrupole-split doublet at 295 K with parameters normal for quintet ($^5T_2$) state iron(II). At 77 K the spectrum is essentially that of a singlet ($^1A_1$) species with a small contribution arising from residual quintet species. Both singlet and quintet species contribute to the spectrum of $[Fe(2mpt)_3][ClO_4]_2$ at 295 K, the low-velocity line of the high-spin doublet overlapping with the lines due to low-spin species. At 77 K a spectrum due only to low-spin species is obtained. The purely high-spin nature of [Fe-

Table VI. Mössbauer Spectral Data for $[FeL_3][ClO_4]_2$

L	T, K	δ_{is}, mm s^{-1}	ΔE_Q mm s^{-1}	spin state
2mpt	295	0.82	0.70	$^5T_2$
2mpt	295	0.49	0.14	$^1A_1$
2mpt	77	0.52	0.34	$^1A_1$
4mpt	295	1.04	1.10	$^5T_2$
4mpt	77	1.19	1.41	$^5T_2$ (minor)
4mpt	77	0.48	0.35	$^1A_1$
6mpt	77	1.18	2.40	$^5T_2$

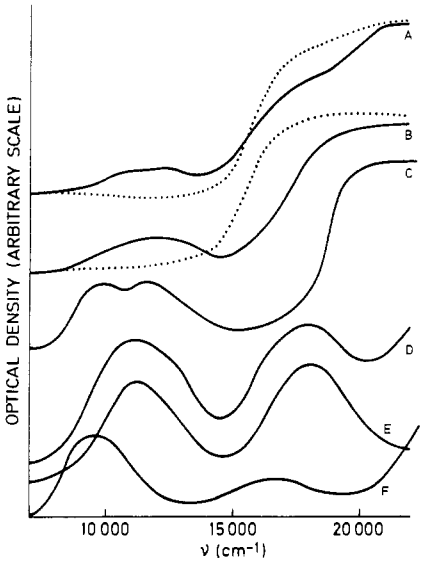

Figure 2. Diffuse reflectance and electronic absorption spectra of iron and nickel complexes: (A) $[Fe(2mpt)_3][ClO_4]_2$ in the solid state (solid line, room temperature; broken line, 77 K); (B) $[Fe(4mpt)_3][ClO_4]_2$ in the solid state (solid line, room temperature; broken line, 77 K); (C) $[Fe(6mpt)_3][ClO_4]_2$ in the solid state at 77 K. (D) $[Ni(4mpt)_3][ClO_4]_2$ (aqueous acetone solution); (E) $[Ni(2mpt)_3][ClO_4]_2$ (aqueous acetone solution); (F) $[Ni(6mpt)_3][ClO_4]_2$ (aqueous acetone solution).

(25) König, E.; Ritter, G.; Kulshreshtha, S. K. *Chem. Rev.* **1985**, *85*, 219.

(26) König, E.; Ritter, G.; Kulshreshtha, S. K.; Goodwin, H. A. *Inorg. Chem.* 1983, *22*, 2518.

(27) Baker, A. T.; Goodwin, H. A. *Aust. J. Chem.* **1977**, *30*, 771.

(28) Sasaki, Y.; Shigematsu, T. *Bull. Chem. Soc. Jpn.* **1973**, *46*, 3438.

Table VII. Spectral Data for $[NiL_3][ClO_4]_2$ (Aqueous Acetone)[a]

L	ν_1, cm^{-1}	ν_2, cm^{-1}	$\nu_2:\nu_1$
2mpt	11 200 (14)	18 000 (16)	1.61
4mpt	11 100 (12)	17 800 (15)	1.62
6mpt	9 600 (27)	16 600 (12)	1.73

[a] Extinction coefficients (L mol^{-1} cm^{-1}) are given in parentheses.

$(6mpt)_3][ClO_4]_2$ at low temperature is confirmed by its Mössbauer spectrum, which shows a single strongly quadrupole-split doublet at 77 K with parameters normal for quintet state iron(II). The parameters are listed in Table VI.

Electronic Spectra. The electronic spectral characteristics for solid $[Fe(2mpt)_3][ClO_4]_2$ and $[Fe(4mpt)_3][ClO_4]_2$ are strongly temperature dependent, as expected for spin-crossover systems. The reflectance spectra for the solid salts are shown in Figure 2. These are dominated by charge-transfer absorption but in addition at 295 K show broad absorption in the range 10 000–14 000 cm^{-1}. This is assigned to components of the $^5T_{2g} \rightarrow {}^5E_g$ transition split by Jahn–Teller and/or low-symmetry effects. At 77 K this absorption disappears, which supports its origin in the quintet species. The charge-transfer absorption becomes more intense and is displaced somewhat to lower energy at low temperature, reflecting the increased population of the singlet state in accord with the $t_{2g} \rightarrow \pi^*$ assignment for this absorption. This change is responsible for the visible darkening of the color of these samples when they are cooled.

$[Fe(6mpt)_3][ClO_4]_2$ is much less intensely colored than the other salts, and the ligand field absorption is well resolved at 77 K. This is centred at 10 800 cm^{-1}, considerably lower energy than that indicated for the two crossover systems. More precise comparison of the ligand field parameters for the three ligands is afforded by the spectra of the nickel(II) complexes $[NiL_3][ClO_4]_2$. These were all measured in aqueous acetone solution and are shown in Figure 2. The ligand field bands are well resolved, and the spectra are typical for essentially octahedral $[NiN_6]^{2+}$ systems. Spectral data are listed in Table VII. The energy of the ν_1 transition is a direct measure of the octahedral field splitting energy and indicates that the order of field strengths is 2mpt > 4mpt > 6mpt. This is consistent with the magnetic data for the corresponding iron complexes. The value for $Dq(Ni^{2+})$ for $[Fe(6mpt)_3][ClO_4]_2$ (960 cm^{-1}) is relatively low and is outside the range found to lead to spin pairing in the corresponding iron(II) complex.[29] The ratio $Dq(Fe^{2+}):Dq(Ni^{2+})$ for the 6mpt complexes is 1.13, which is in good agreement with values reported for ligands whose field strengths are close to the iron(II) crossover value.[29] Both the methylthiazole derivatives 2mpt and 4mpt provide weaker fields than the unsubstituted species, as would be expected on steric grounds, but for both substituted and unsubstituted species the 4-(pyridin-2-yl)thiazole derivative provides the stronger field.[15,16]

Structural Data. The structure of $[Fe(4mpt)_3][ClO_4]_2$ was determined at both 294 and 133 K. This species was chosen for structural study since it displays an almost complete and fairly sharp transition within this range, thus allowing for characterization of the two spin isomers. In addition the structure of $[Ni(4mpt)_3][ClO_4]_2$ was determined so as to allow meaningful comparisons of the ligand bonding characteristics without any influence of the metal ion spin state.

The crystals for the three structure determinations are isostructural in space group $P\bar{3}c1$ (No. 165) with the metal atom at the 32 site at $0,0,^1/_4$ and each 2-fold axis running through the unsymmetrical bidentate ligand necessarily imposing disorder. An ordered structure in $P3c1$ (No. 158) was excluded by its inferior refinement. Complete hemispheres of data were collected and confirmed the $\bar{3}m$ diffraction symmetry. For the iron complex at 294 K and for the nickel complex the perchlorate ions that separate columns of the cations were found to be disordered about the 3-fold axis at $^1/_3$, $^2/_3$, z in a way not directly attributable to a center of inversion. For the iron complex at 133 K the anions

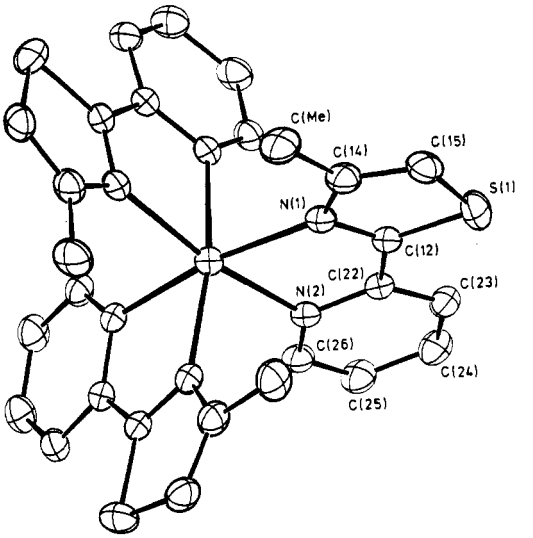

Figure 3. View of $[Fe(4mpt)_3]^{2+}$ down the c axis. The atom-labeling scheme is common to all three structures.

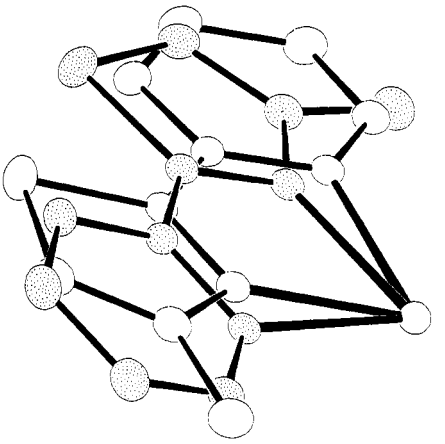

Figure 4. View down the c axis showing the overlap of the two orientations of the ligand for $[Fe(4mpt)_3][ClO_4]_2$.

are oriented in such a way that a 3-fold axis of the ClO_4 tetrahedron is coincident with the crystallographic 3-fold axis. This implies a disorder–order transition that is discussed later.

A view of the $[Fe(4mpt)_3]^{2+}$ ion at 294 K is shown in Figure 3. The atom labelling scheme is common to all three structures. The cation shown has the *facial* configuration. Since there are two possible orientations for each ligand, there are eight possible configurations for the cation. If orientation A is defined as pyridinyl ring *down* and orientation B as pyridinyl ring *up*, then the configuration of the cation shown in Figure 3 is AAA. Other possible configurations are AAB, ABA, ABB, etc., all of which are equally likely on statistical grounds. The ratio of *mer* to *fac* isomers should thus be 3:1, but the structure determinations give no information about the actual ratio. Ligand–ligand steric interaction due to the methyl substituents would be reduced in the *mer* isomer, and thus the cation would be expected to have this structure, as does $[Fe(2\text{-mephen})_3]^{2+}$.[10]

Convergence of the refinement was obtained by applying constraints. However, consistency of ligand structures for the three determinations was not obtained. Initially no bond length constraints were imposed in an endeavor to investigate the ability of rigid-body thermal parametrization (TLX) together with planarity constraints to resolve completely correlation between positional and thermal parameters to describe overlapped atoms.

The two orientations of the ligand are extensively overlapped (see Figure 4). For example, for the iron complex at room temperature the distances between N(2) and N(1) $(y, x, ^1/_2 - z)$ is 0.53 Å and that between C(Me) and C(26) is 0.68 Å. In this event, the correlation problems between the positional and thermal parameters still remain. After initial convergence, weighted

(29) Robinson, M. A.; Curry, J. D.; Busch, D. H. *Inorg. Chem.* **1963**, *2*, 1178.

Table VIII. Weighted Average Intraligand Distances (Å) for $[M(4mpt)_3][ClO_4]_2$

bond	dist	bond	dist
N(1)–C(12)	1.326	C(22)–N(2)	1.324
N(1)–C(14)	1.358	C(22)–C(23)	1.398
C(12)–S(1)	1.687	C(23)–C(24)	1.361
S(1)–C(15)	1.708	C(24)–C(25)	1.373
C(14)–C(15)	1.353	C(25)–C(26)	1.357
C(14)–C(Me)	1.467	C(26)–N(2)	1.317
C(12)–C(22)	1.460		

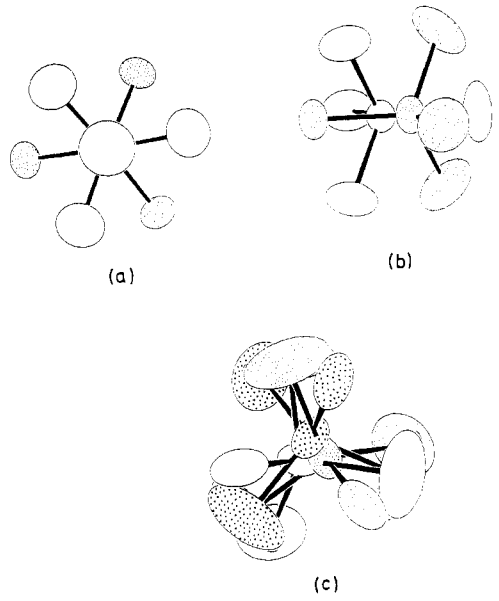

Figure 5. View of the anion of $[Fe(4mpt)_3][ClO_4]_2$: (a) down the *c* axis at 133 K; (b) down the *b* axis at 133 K; (c) down the *c* axis at 294 K showing the disorder. One oxygen atom for each equivalent position is obscured.

average intraligand distances (d_{av}) were determined by using $1/\sigma^2$ as weights where σ is the estimated standard deviation for each distance in each structure:

$$d_{av} = \frac{d_1(1/\sigma_1^2) + d_2(1/\sigma_2^2) + d_3(1/\sigma_3^2)}{1/\sigma_1^2 + 1/\sigma_2^2 + 1/\sigma_3^2}$$

The average distances obtained by this procedure are listed in Table VIII. It is noted that N(2)–C(26) is only 1.317 Å, much shorter than the expected C–N bond length for a pyridine ring. As mentioned previously, C(26) is close to the alternative orientation of C(Me) and N(1) is close to N(2). Since the interference between these sites is common to all three determinations, the averaging procedure will not improve the situation. In subsequent refinement, intraligand distances were restrained to these average values, and no discernible difference in agreement factors resulted. The separation of the nitrogen atoms in the alternate orientations is a vector essential perpendicular to the metal–nitrogen bonds. As a consequence the metal–nitrogen bond lengths are quite reliable. The structure of the thiazole ring is typical for coordinated thiazole ligands and reveals the conjugated diimine sequence, N–C–C–N–, in the bidentate. Coordination of the thiazole moiety is via the nitrogen atom, despite the position of the methyl substituent.

Two views of the anion of $[Fe(4mpt)_3][ClO_4]_2$ at 133 K are shown in Figure 5. At 294 K the anion is disordered as shown in Figure 5c. The atomic positions shown are not an entirely successful model as the contributions of residual electron density to each reflection were removed from the data to allow further refinement of the remainder of the structure. More realistic error estimates for the cation were thus obtained. Obviously a disorder–order transition involving the perchlorate ion occurs between 294 and 133 K. The terms order and disorder are being used relatively; the anion has two orientations at 133 K but this is certainly more ordered than in the high-temperature structure.

Table IX. Bond Angles (deg) for $[M(4mpt)_3][ClO_4]_2$

	M		
angle	Ni	Fe(294 K)	Fe (133 K)
N(1)–M–N(2)	78.6 (2)	76.6 (2)	80.8 (4)
M–N(1)–C(12)	111.4 (5)	112.3 (4)	111.5 (9)
M–N(1)–C(14)	138.2 (6)	138.3 (5)	137.9 (12)
C(12)–N(1)–C(14)	110.5 (8)	109.4 (7)	110.5 (15)
C(12)–S(1)–C(15)	89.6 (4)	90.0 (3)	90.4 (7)
C(22)–C(12)–N(1)	120.5 (7)	120.1 (6)	119.3 (14)
C(22)–C(12)–S(1)	124.8 (5)	124.8 (5)	126.6 (10)
N(1)–C(12)–S(1)	114.7 (5)	115.0 (4)	114.1 (10)
N(1)–C(14)–C(15)	115.0 (9)	116.5 (7)	115.7 (16)
N(1)–C(14)–C(Me)	119.4 (8)	119.2 (7)	120.4 (15)
C(15)–C(14)–C(Me)	125.4 (8)	124.2 (6)	123.8 (14)
S(1)–C(15)–C(14)	110.3 (7)	109.1 (6)	109.4 (12)
M–N(2)–C(22)	113.6 (5)	113.4 (4)	114.4 (10)
M–N(2)–C(26)	128.4 (6)	128.5 (5)	130.5 (11)
C(22)–N(2)–C(26)	117.0 (8)	116.8 (6)	114.2 (16)
N(2)–C(22)–C(23)	122.3 (7)	120.4 (6)	121.8 (15)
N(2)–C(22)–C(12)	114.8 (7)	116.1 (6)	113.0 (14)
C(23)–C(22)–C(12)	122.9 (7)	123.5 (6)	125.2 (16)
C(22)–C(23)–C(24)	118.4 (8)	121.4 (7)	121.5 (19)
C(23)–C(24)–C(25)	119.4 (7)	117.5 (7)	117.0 (17)
C(24)–C(25)–C(26)	117.4 (7)	117.3 (6)	116.8 (15)
N(2)–C(26)–C(25)	125.3 (8)	126.6 (8)	128.7 (16)

Table X. Metal–Donor Atom Distances (Å) for $[M(4mpt)_3][ClO_4]_2$

M	$M–N_{pyridine}$	$M–N_{thiazole}$
Fe(294 K)	2.199 (7)	2.183 (7)
Fe(133 K)	2.040 (10)	2.028 (9)
Ni	2.134 (8)	2.118 (9)

Order–disorder structural transitions have been detected in other systems displaying electronic spin transitions, and questions arise whether the two transitions are associated and whether one actually triggers the other. The spin transition in $FeCl_2(Ph_2PCH{=}CHPPh_2)_2{\cdot}2(CH_3)_2CO$ is relatively gradual, and the solvate acetone molecules order into two orientations over a wide temperature range as the temperature is lowered.[30] It is suggested in this instance that the disorder–order transition triggers the spin transition since both transitions are centered at about the same temperature and follow a gradual course. This was deduced from a detailed study of the temperature dependence of the Mössbauer spectral line widths. A more obvious rationale for cooperativity between the spin and the disorder–order transitions is provided by structural data for $[Fe(pic)_3]Cl_2{\cdot}EtOH$ (pic = 2-picolylamine). In this, the ordering of the ethanol molecules changes the relative strengths of hydrogen bonding in the network linking the cation, anions, and solvate molecules and results in an increase in electron density on the amino nitrogen atoms, thereby initiating the spin change.[14] For $[Fe(bi)_3][ClO_4]_2$ (bi = 2,2′-biimidazoline) on the other hand, the spin transition and the disorder–order transition are distinctly separated.[31] For the system of the present work it is not possible without further detailed study to link directly the anion-orientational and spin transitions.

Bond angles are listed in Table IX, and the metal–donor atom distances are listed in Table X. For the nickel complex the metal–donor atoms distances are all greater than those observed in previously studied related systems ($[Ni(bpy)_3]^{2+}$, Ni–N = 2.089;[32] $[Ni(4bt)_3]^{2+}$, Ni–N = 2.082;[33] $[Ni(4pt)_3]^{2+}$ $Ni–N_{(py)}$ = 2.108, $Ni–N_{(th)}$ = 2.056 Å[16]). This indicates a definite steric effect from the methyl substituent is operative, and the nickel–donor atom distances are in accord with the trend in ligand field parameters for the series of ligands.

The data in Table X indicate that the $M–N_{thiazole}$ distances are consistently shorter than the $M–N_{pyridine}$ distances but the dif-

(30) König, E.; Ritter, G.; Kulshreshtha, S. K.; Waigel, J.; Sacconi, L. *Inorg. Chem.* **1984**, *23*, 1241.
(31) König, E.; Ritter, G.; Kulshreshtha, S. K.; Nelson, S. M. *Inorg. Chem.* 1982, *21*, 3022.
(32) Finney, A. J.; Hitchman, M. A.; Kepert, D. L.; Raston, C. L.; Rowbottom, G. L.; White, A. H. *Aust. J. Chem.* **1981**, *34*, 2177.
(33) Baker, A. T.; Goodwin, H. A. *Aust. J. Chem.* **1985**, *38*, 851.

Table XI. Distances (Å) of the Metal Atom out of the Planes Defined by the Heterocyclic Rings for $[M(4mpt)_3][ClO_4]_2$

M	pyridinyl ring	thiazolyl ring
Fe(294 K)	−0.422	0.018
Fe(133 K)	−0.313	0.021
Ni	−0.362	0.008

Table XII. Normalized Bite (b) and Trigonal Twist Angle (θ) for $[M(4mpt)_3][ClO_4]_2$

M	b, deg	θ, deg
Fe(294 K)	1.24	24.8
Fe(133 K)	1.30	27.5
Ni	1.27	26.0

ference is in no case significant ($<3\sigma$). It is perhaps surprising, nevertheless, that this trend should be indicated since the methyl group would be expected to be hindering the coordination of the thiazole nitrogen in particular. In the unsubstituted 4-(pyridin-2-yl)thiazole complex the same effect is observed,[16] and even in the tris(4,4′-bithiazole)nickel(II) ion the bond lengths are shorter than those in the tris(2,2′-bipyridine)nickel(II) ion.[33] It is noteworthy that for all three structures of the present work the metal atom is further out of the plane defined by the pyridine ring than that of the thiazole. The distances are given in Table XI. This all suggests that the relevant orbitals in the thiazole are more favorable than those on the pyridine moiety for overlap with the metal orbitals.

Magnetic data indicate that at 133 K the iron complex is approximately 92% low spin. When allowance is made for the small high-spin fraction at 133 K, the difference in Fe–N distance in the pure high-spin and the pure low-spin species is estimated to be 0.17 Å. This is fairly typical for iron(II) spin transition systems. The actual Fe–N distance (average) estimated for the pure low-spin species (2.02 Å) is significantly longer than that found in $[Fe(bpy)_3]^{2+}$ or $[Fe(4pt)_3]^{2+}$,[33,34] indicating that the steric effect noted in the nickel complex is operative in the low-spin iron complex too. The average $Fe–N_{thiazole}$ distance in the quintet state species at 294 K is significantly shorter than the average Fe–N-(CH_3) distance (2.25 Å) in $[Fe(mephen)_3]^{2+}$,[10] indicative of the greater steric effect of the substituent in the six-membered ring.

In the structure determinations no constraints were applied regarding the angle between the planes defined by the two heterocyclic rings of the ligand molecules. The relevant dihedral and N(1)–C(12)–C(22)–N(2) torsional angles are 9.3 and −9.1° (Fe at 294 K), 7.3 and −6.0° (Fe at 133 K), and 7.9 and −6.0° (Ni). The similarity in the respective dihedral and torsional angles indicates that the twist between the two rings is confined essentially to the chelate ring.

The distortions present in the metal ion environment in these complexes may be defined in terms of the parameters *normalized bite* (b) and *trigonal twist angle* (θ) developed by Kepert,[35] who has established an empirical relationship between b and θ. The experimental values for b and θ are listed in Table XII. The values of θ determined are closer to the octahedral limit than predicted ($\theta = 30°$ for regular octahedral stereochemistry; $\theta = 0$ for trigonal stereochemistry), and in this respect the present structures are typical for heterocyclic diimine derivatives. The deviation can be associated with interligand repulsions arising from the substituents adjacent to the donor atoms. These repulsions are reduced in the octahedral stereochemistry.[36]

Solution Studies of the Spin Transition. Magnetic data (Table V) indicate that $[Fe(2mpt)_3][ClO_4]_2$ displays a spin transition in acetone solution, but $[Fe(4mpt)_3][ClO_4]_2$ remains high spin under the same conditions. The solution behavior of the former may be treated as a genuine LS ⇌ HS (low-spin ⇌ high-spin) equilibrium and values for the equilibrium constant (K = [HS]/[LS]) at various temperatures may be extracted from the magnetic data by assuming values of 5.4 and 0.7 μ_B for the pure high-spin and low-spin species, respectively. The resulting plot of ln K vs. $1/T$ is linear, and from this the thermodynamic parameters ΔH = 29 kJ mol^{-1} and ΔS = 120 J K^{-1} mol^{-1} were obtained. These values are at the upper end of the range usually found for iron(II) systems in solution. The high value for ΔS for the present system, as compared with values obtained for transitions in solid samples,[25] lends support to the view that the major entropic term arises from outer-sphere reorganization, which would be more significant in the solution phase.

Although no crystallographic data are available for $[Fe(2mpt)_3]^{2+}$, its structure would not be expected to be too different from that of $[Fe(4mpt)_3]^{2+}$ and the changes in bond lengths within the coordination sphere accompanying the spin transition should be similar for the two systems. On the basis of the bond length changes observed for $[Fe(4mpt)_3][ClO_4]_2$, a qualitative estimate of the inner-sphere reorganization energy can be made[37] and a value in the range 20–26 kJ mol^{-1} is predicted. This indicates, then, that this inner coordination sphere rearrangement is the major factor determining the enthalpic term associated with the spin change.

The systems reported in the present work provide new examples illustrating several of the general features associated with the manifestation of spin transitions in iron(II). These include the somewhat reduced steric barrier to coordination and thereby to spin pairing caused by a substituent adjacent to a donor atom in a five-membered ring, compared with one in a six-membered ring, the rather large contraction in the metal–donor atom distance that accompanies conversion from a high-spin to a low-spin state, and the possible association of order–disorder transitions with spin transitions in solid samples. The frequently noted influences of solid-state effects is illustrated by the varying degrees of continuity noted in the course of the spin transitions, in the influence of associated counterions, and in a lack of consistency in the behavior of the systems in the solid state and in solution. Finally, this work confirms the significantly stronger coordinating capacity of 4-(pyridin-2-yl)thiazole derivatives compared with that of the corresponding 2-substituted species.

Acknowledgment. Financial support from the Australian Research Grants Scheme and the assistance of Dr. H. Pham in obtaining the microanalyses are gratefully acknowledged.

Registry No. **3**, 110095-86-8; $[Fe(\mathbf{1})_3][BF_4]_2$, 110095-76-6; $[Fe(\mathbf{1})_3][ClO_4]_2 \cdot H_2O$, 110095-78-8; $[Ni(\mathbf{1})_3][ClO_4]_2$, 110095-83-5; $[Fe(\mathbf{2})_3][ClO_4]_2$, 110095-71-1; $[Fe(\mathbf{2})_3][BF_4]_2$, 110095-74-4; $[Ni(\mathbf{2})_3][ClO_4]_2$, 110095-73-3; $[Fe(\mathbf{3})_3][ClO_4]_2 \cdot H_2O$, 110095-81-3; $[Ni(\mathbf{3})_3][ClO_4]_2$, 110095-85-7; 6-methyl-2-thiopicolinamide, 5933-30-2; bromoacetal, 2032-35-1.

Supplementary Material Available: Tables SI–SV, listing analytical data and thermal parameters for $[Fe(4mpt)_3][ClO_4]_2$ at 294 and 133 K and thermal parameters and positional parameters for hydrogen atoms for $[Ni(4mpt)_3][ClO_4]_2$ (5 pages); Tables SVI–SVIII, listing calculated and observed structure factors for $[Fe(4mpt)_3][ClO_4]_2$ at 294 and 133 K and for $[Ni(4mpt)_3][ClO_4]_2$ (11 pages). Ordering information is given on any current masthead page.

(34) Garcia Posse, M. E.; Juri, M. A.; Aymonino, O. E.; Piro, O. E.; Negri, H. A.; Castellano, E. E. *Inorg. Chem.* **1984**, *23*, 948.
(35) Kepert, D. L. *Prog. Inorg. Chem.* **1977**, *23*, 1.
(36) Goodwin, H. A.; Kepert, D. L.; Patrick, J. M.; Skelton, B. W.; White, A. H. *Aust. J. Chem.* **1984**, *37*, 1817.
(37) Dose, E. V.; Hoselton, M. A.; Sutin, N.; Tweedle, M. F.; Wilson, L. J. *J. Am. Chem. Soc.* **1978**, *100*, 1141.